AGU PUBLICATIONS

Radio Science

RESEARCH ARTICLE
10.1002/2016RS006061

Key Points:
- Turbulence acting on EM propagation loss can be modeled by adding fluctuations to a forward propagation loss model at discrete range steps
- Atmospheric refractivity profile estimation is not as accurate as previously thought when considering randomness introduced by turbulence
- A genetic algorithm can be used to invert for a height-varying refractivity profile given propagation loss measurements over range

Correspondence to:
M. Wagner,
m2wagner@eng.ucsd.edu

Citation:
Wagner, M., P. Gerstoft, and T. Rogers (2016), Estimating refractivity from propagation loss in turbulent media, *Radio Sci.*, *51*, doi:10.1002/2016RS006061.

Received 18 APR 2016
Accepted 18 NOV 2016
Accepted article online 24 NOV 2016

Estimating refractivity from propagation loss in turbulent media

Mark Wagner[1], Peter Gerstoft[1], and Ted Rogers[2]

[1]University of California, San Diego, San Diego, California, USA, [2]SPAWAR, San Diego, California, USA

Abstract This paper estimates lower atmospheric refractivity (M-profile) given an electromagnetic (EM) propagation loss (PL) measurement. Specifically, height-independent PL measurements over a range of 10–80 km are used to infer information about the existence and potential parameters of atmospheric ducts in the lowest 1 km of the atmosphere. The main improvement made on previous refractivity estimations is inclusion of range-dependent fluctuations due to turbulence in the forward propagation model. Using this framework, the maximum likelihood (ML) estimate of atmospheric refractivity has good accuracy, and with prior information about ducting the maximum a priori (MAP) refractivity estimate can be found. Monte Carlo methods are used to estimate the mean and covariance of PL, which are fed into a Gaussian likelihood function for evaluation of estimated refractivity probability. Comparisons were made between inversions performed on propagation loss data simulated by a wide angle parabolic equation (PE) propagation model with added homogeneous and inhomogeneous turbulence. It was found that the turbulence models produce significantly different results, suggesting that accurate modeling of turbulence is key.

1. Introduction

Refractivity of a medium represents the amount which an electromagnetic (EM) wave will bend while propagating through the medium. Atmospheric refractivity is of particular interest because there exist common height-varying refractivity profiles, which act as waveguides for EM waves, known as ducts. The atmospheric inversion layer is primarily responsible for ducts and separates the colder and more humid mixed layer from the free troposphere; thus, there exists a large negative humidity gradient. Turbulence in the inversion layer will cause more humidity variation in that layer relative to other layers. This will cause more refractivity fluctuations in the inversion layer.

Ducting is a naturally occurring event that is known to cause anomalies in long range EM equipment. Examples of these anomalies include unusually long operational range or increased clutter in return signals. For operators of EM equipment it is beneficial to know when a ducting phenomenon is occurring to better understand the possible effects on system performance. Thus, it is desirable to have some way to characterize the qualities of a duct from simple measurements. Because it is known that variation in atmospheric refractivity causes variation in PL measurements [*Lentini and Hackett*, 2015], it may be possible to infer a refractivity profile from PL.

From a range-independent refractivity profile parameterized by $\mathbf{m}$ (defined in section 2.1), a deterministic matrix of PL over height and range can be computed from a forward model $F(\mathbf{m})$ (defined in section 3). The parabolic equation (PE) method is used for this calculation [*Craig and Levy*, 1991]. The forward model can be used to find the appropriate M-profile that statistically best recreates a measured PL.

Turbulence, parameterized by C_n^2, causes random fluctuations in refractivity [*Wesely*, 1976], which in turn propagate through the forward model, $F\left(\mathbf{m}, C_n^2\right)$ resulting in fluctuations in PL obeying an unknown distribution. C_n^2 is a parameter relating to the magnitude of fluctuations in refractivity from atmospheric turbulence. Stochastic variation in the forward model is expected to increase with range due to the compounding effect of fluctuations as they propagate forward [*Barrios*, 2008]. As a result, even small perturbations in refractivity can lead to large changes in PL at longer distances.

For inversion, the effects of turbulence mean:

1. The forward model for PL, $F\left(\mathbf{m}, C_n^2\right)$, is now stochastic. As a result, a means to calculate an average PL vector given $\mathbf{m}$ and C_n^2 becomes important.

2. The fluctuations in refractivity will have an effect on fluctuations in PL. The distribution of refractivity fluctuations must be modeled, as well as the distribution of the resulting fluctuations in PL.
3. The uncertainty in the PL vector increases with range. In previous inversions [*Gerstoft et al.*, 2003; *Yardim et al.*, 2006, 2007, 2009] uncertainty was assumed range independent, an assumption which does not hold when turbulence is present. This time, a full covariance matrix of PL, $\mathbf{C}_d$, must be calculated to find the likelihood of a measurement given $\mathbf{m}$ and C_n^2.

This work attempts to build upon previous efforts to estimate refractivity from clutter [*Karimian et al.*, 2011; *Douvenot et al.*, 2008; *Gerstoft et al.*, 2003] with the added component of randomness from atmospheric turbulence. The primary goals are to find an accurate method of modeling turbulence and to describe the effect on refractivity estimations.

2. Theory

2.1. Refractivity

Bending of the propagation path of an electromagnetic wave due to variation in the speed of light is known as refraction and is the cause of ducting phenomenon. The refractive index n is defined as

$$n = c/v\,, \tag{1}$$

where c is the speed of light in vacuum and v is the speed of light in the medium being propagated through. Near the Earth's surface n is typically 1.000350. Because n is close to unity, another variable N known as refractivity is adopted for clarity

$$N = (n-1)\times 10^6\,. \tag{2}$$

Atmospheric refractivity is a function of temperature T, pressure P, and partial water vapor e.

$$N = 77.6\left[P/T + 4810e/T^2\right]\,, \tag{3}$$

where P and e are measured in hectopascals (hPa) and T in kelvin (K). When tracking the height of propagating electromagnetic waves over the Earth's surface, it becomes necessary to account for the curvature of the Earth. A variable M, modified refractivity, is defined to transform the Earth to a flat surface:

$$M = N + (h/a)\times 10^6 = N + .157h\,, \tag{4}$$

where h is height above Earth's surface and a is the radius of the Earth in kilometers.

In the radar community, atmospheric ducts are represented by a refractivity profile which varies with height but is often assumed range independent. A sample M-profile representing the case where both an evaporation and surface-based duct exists is shown in Figure 1. It is only necessary to know a few deterministic parameters of a refractivity profile for adequate description of the propagation environment [*Rogers*, 1998], so we limit description of the refractive environment to five variables organized into vector $\mathbf{m}$, with elements m_i representing the ith parameter. From $\mathbf{m}$ all realistic M-profiles can be constructed. The five parameters are shown in Figure 1.

An M-profile can be generated from $\mathbf{m}$ and used as input to the forward model, which is an electromagnetic wide angle split step fast Fourier transform PE [*Barrios*, 1992; *Levy*, 2000]. The forward model is set with parameters of the wave in question which includes transmitter height, max range of propagation, frequency, height and range step size, height of measurement, and maximum propagation angle (and will later also take in turbulence structure coefficient of the atmosphere, C_n^2). The forward model calculates PL of the specified wave over height and range. Because realistic measurements of PL are generally taken at one height, only the height of measurement is kept. This height is an internal parameter of the model which can be altered to match the situation being simulated. The output, $F(\mathbf{m})$, of the forward model is an N_f dimensional vector corresponding to the theoretical propagation loss at the given height.

2.2. Turbulence

When the forward model $F(\mathbf{m})$ is run, a deterministic output is generated which can be exactly recomputed given an identical input $\mathbf{m}$. In reality, the propagation pattern of an EM wave through a steady duct shows

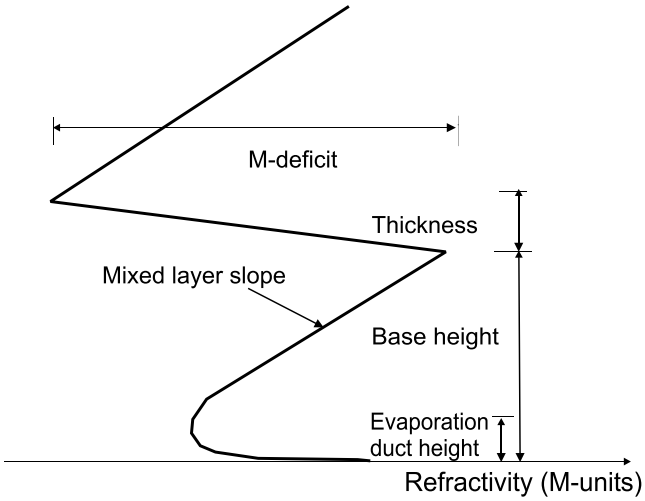

Figure 1. Refractivity profile representing a ducting phenomenon.

short-term fluctuations. This is because turbulence causes atmospheric variables such as temperature, pressure, and vapor pressure to fluctuate constantly, which in turn cause the mean refractivity profile to fluctuate constantly and results in the scattering of waves propagating through the atmosphere [*Wilson et al.*, 1999]. This section adds stochastic fluctuations to the refractivity profile so that the forward model can realistically reflect randomness introduced by turbulence.

2.2.1. Stochastic Elements of Refractivity

It is assumed that the M-profile is subject to continuous fluctuations due to atmospheric turbulence. To model fluctuations in refractivity due to turbulence, the refractivity profile is split into two parts: the range-independent mean refractivity $\langle n(z)\rangle$ and a stochastically fluctuating part $\tilde{n}(x,z)$.

$$n(x,z) = \langle n(z)\rangle + \tilde{n}(x,z)\,. \tag{5}$$

where $\langle\cdot\rangle$ represents mean. While $\langle n(z)\rangle$ is deterministic and can be fully specified by **m**, $\tilde{n}(z)$ is stochastic and requires a spectrum to generate realizations.

2.2.2. Structure Function

The structure function is defined as the covariance of the difference of a process between position vector r and $r + \Delta r$ where Δr is a displacement vector from starting location r [*Wyngaard and LeMone*, 1980].

$$D_n(r,\Delta r) = \left\langle [n(r) - n(r+\Delta r)]^2 \right\rangle \tag{6}$$

where $n(r)$ is the refractivity at point r. If we assume that the structure function is identical from all starting positions and orientations (which is the assumption of local homogeneity), then equation (6) becomes a functions of just $\mathbf{r} = |\Delta r|$. Local homogeneity is an assumed in Kolmogorov's second similarity hypothesis [*Kolmogorov*, 1941]. Using dimensional analysis, it was concluded that the structure function of a medium-scale turbulent field is a function of distance **r** from the starting location and obeys

$$D_n(\mathbf{r}) \propto C_n^2 \mathbf{r}^{2/3} \tag{7}$$

where C_n^2 is the structure function constant of the subscripted variable n and represents the magnitude of $\tilde{n}(z)$. Note that (7) applies only to medium-scale fluctuations. Structure functions of large- and small-scale fluctuations are modeled by different equations because the shape of their spectrums is modeled differently than that of medium-scale fluctuations [*Pope*, 2000].

Equation (7) is known as the simplified Kolmogorov's 2/3 law and condenses all unknowns into the structure function constant C_n^2. The structure function constant can be obtained from physical measurement; however, it is known that its value changes with height above the boundary layer. We initially assume height independence of C_n^2 to preserve the assumption of homogeneity. Later we redact this assumption and observe the effect on the accuracy of our inversion.

2.2.3. Modeling Turbulence

We choose a robust spectral model that has been used in similar studies known as the von Karman spectrum, visualized in Figure 2.

$$S_n(\kappa) = .033 C_n^2 \left(\kappa^2 + L_0^{-2}\right)^{-11/6} \exp\left(-\kappa^2/\kappa_m^2\right), \tag{8}$$

where κ represents wave number, $\kappa_m = 5.92/l_0$ (known as the inner-scale wave number parameter), l_0 is the boundary between medium- and small-scale fluctuations, and L_0 is the boundary between large- and

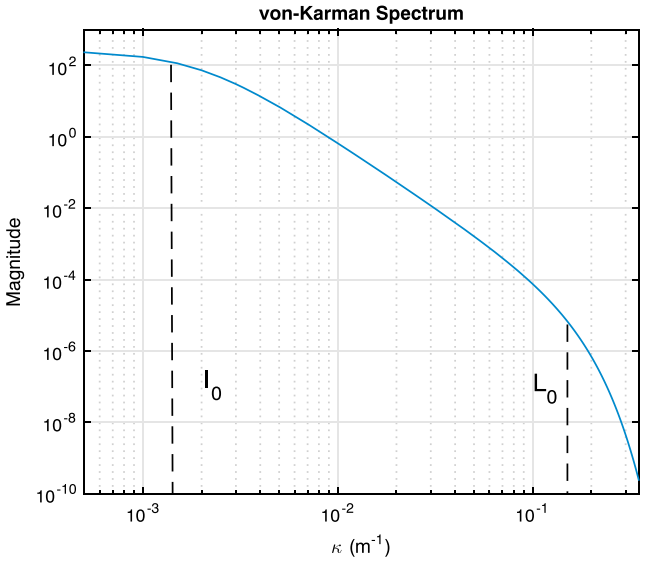

Figure 2. von Karman spectrum divided into large-, medium-, and small-scale subranges.

medium-scale fluctuations known as the integral length scale. The major advantage of the von Karman spectrum is that it approximates Kolmogorov's power law for spatial frequencies $L_0^{-1} < \kappa < l_0^{-1}$ and allows for tuning at other wave numbers. The von Karman spectrum is attractive for its simplicity; however, the algorithm is robust enough that it may be replaced for more accurate spectral models if desired. Additionally, the assumption of homogeneous turbulence in the marine boundary layer is less accurate [*Chamecki and Dias*, 2004] and will be addressed in section 2.3.

Realizations of $\tilde{n}(z)$ are found using [*Percival*, 1993]. An approximate realization U_z of the M point spectrum $S_n(\kappa)$ can be generated using the equation

$$\tilde{n}(z) = U_z = \frac{1}{\sqrt{M}} \sum_{k=0}^{M-1} U_k \exp^{-j2\pi\epsilon_k z} \tag{9}$$

where $\epsilon_k = \frac{k}{M}\epsilon_{\max}$, $\epsilon_{\max}$ is the Nyquist spatial frequency of the desired signal, $j = \sqrt{-1}$, and U_k is defined as

$$U_k = \begin{cases} \sqrt{S_n(0)}W_0, & k = 0 \\ \sqrt{\frac{1}{2}S_n\left(\epsilon_k\right)}\left(W_{2k-1} + jW_{2k}\right), & 1 \le k < \frac{M}{2} \\ \sqrt{S_n\left(\epsilon_{\max}\right)}W_{M-1}, & k = \frac{M}{2} \\ U_k = U_{M-k}^*, & \frac{M}{2} < k \le M-1 \end{cases} \tag{10}$$

Here S_n is the spectrum from which the realizations must match, and W_k is the kth element of a sequence drawn from a Gaussian $N(0, 1)$. Intuitively, (10) is creating a signal which is the product of Gaussian noise and an envelope spectrum which will have a purely real inverse Fourier transform. Equation (9) simply transforms the end result of (10) to a vector which is considered an accurate realization of turbulent noise over height. In practice we generate many independent realizations of $\tilde{n}(z)$ which are used to model turbulence over a large-scale two-dimensional grid representing height and range. Forward model runs of PL with and without turbulent noise are shown is Figure 3.

2.3. Inhomogeneous Turbulence

The marine atmospheric boundary layer (MABL) is a turbulent stratified flow. When fully developed, it consists of a surface layer, mixed layer, and an entrainment zone (often an inversion layer) under the free troposphere. The pressure gradients and geostrophy in the free troposphere produce the wind forcing on the boundary layer. The MABL is evolving continuously in time and space (e.g., a continuous injection of moisture from ocean surface evaporation, radiant heating, and cooling). However, the rate of change in the horizontal is much less than in the vertical. If the mass of a MABL layer is constant, the horizontal pressure gradient and the stresses at each interface sum to zero. The stress at the ocean arises from the friction between the surface layer and the ocean. Above that, combinations of stability and shear provide the balance of stresses and the horizontal pressure gradient at each layer. Higher stability (associated with a positive virtual potential temperature gradient) dampens turbulence, while more shear gives more turbulence. The mixed layer is (nearly) neutrally stable and with low shear, but in the inversion layer both stability and shear are much larger. The point is that turbulence in the inversion layer might not be greater or smaller than in the mixed layer.

Eddies, however, displace particles such that air samples at a given height have a distribution of water vapor content corresponding to the horizontal mean properties of the air at nearby heights. Thus, the stronger the magnitude of water vapor gradient, the larger the variance of the water vapor at that height. Since water

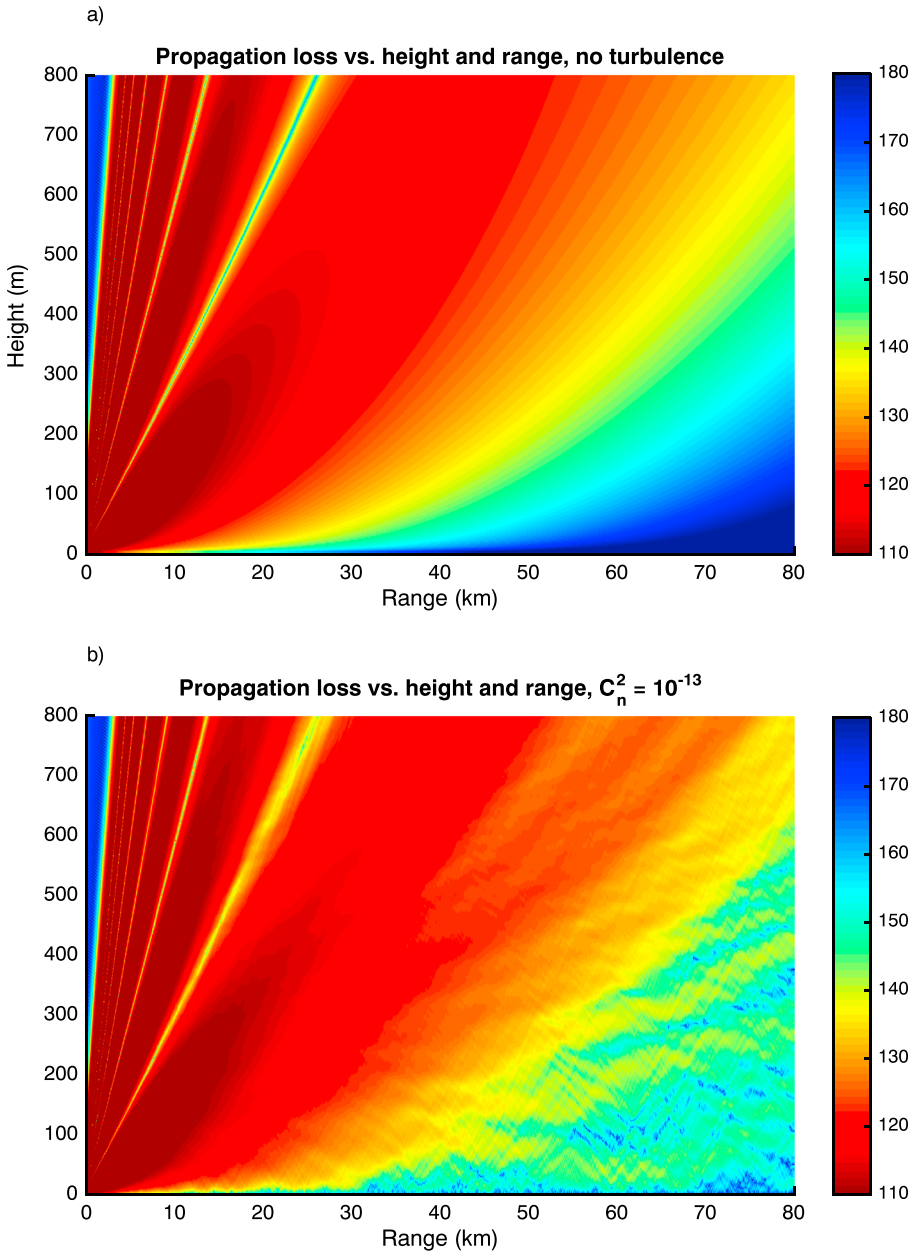

Figure 3. Propagation loss (PL) at 1 GHz propagating through standard atmosphere refractivity profile over height and range, (a) without turbulence and (b) with turbulence parameterized by $C_n^2 = 10^{-13}$.

vapor is the dominant term in the refractivity, the variability of refractivity can be much larger in the inversion layer than in the mixed layer.

Use of numerical simulation techniques such as large eddy simulation (LES) *Gilbert et al.* [1999] has shown that the magnitude of $\tilde{n}(z)$ can increase more than tenfold near the inversion layer of a duct. This implies that C_n^2 varies over height when a duct is present, hitting a maximum in the middle of the inversion layer and returning to a nearly constant value above the duct. We attempt to model fluctuations subject to height-varying $C_n^2(z)$ and refer to turbulence generated under this model as inhomogeneous turbulence.

A simulation of inhomogeneous turbulence was conducted by changing C_n^2 from a constant value to a function of height, $C_n^2(z)$, then generating corresponding realizations of $\tilde{n}(z)$. A simple formula was created for $C_n^2(z)$ which models an increase in C_n^2 around the middle of a ducts inversion layer.

$$C_n^2(z) = C_s\left[1 + K\exp\left(\frac{-\left(z-\left(m_3+\frac{m_4}{2}\right)\right)^2}{\left(\frac{m_4}{2}\right)^2}\right)\right] \tag{11}$$

where C_s represents the reference value of C_n^2, m_3 and m_4 are the base height and thickness of the duct respectively, and K can be adjusted to give any desired maximum to the function $C_n^2(z)$. Equation (11) creates a C_n^2 profile which increases $(1+K)$ fold at the inversion layer. Realizations of height dependent inhomogeneous turbulence, $n_{\text{ih}}(z)$, following (11) are generated as follows,

$$n_{ih}(z) = \tilde{n}(z)\left[1 + K\exp\left(\frac{-\left(z-\left(m_3+\frac{m_4}{2}\right)\right)^2}{\left(\frac{m_4}{2}\right)^2}\right)\right] \tag{12}$$

where $n_f(z)$ is generated using $C_n^2 = C_s$. It has been shown that (12) produces accurate realizations of $n_{\text{ih}}(z)$ [*Rouseff*, 1992] if the medium can be assumed quasi homogeneous, an assumption which is popular in similar wave propagation studies [*Ishimaru*, 1978], [*Tatarskii*, 1971].

For inversions in the preceding examples, (12) is used to generate inhomogeneous turbulence with $K=9$ to achieve a tenfold increase in C_n^2 at the inversion layer. The increase in C_n^2 makes refractivity fluctuations larger just below the duct interface by increasing turbulent fluctuations. *Gilbert et al.* [1999] suggest that this is more consistent with reality than constant $C_n^2(z)$. The forward model was run on two refractivity profiles with identical parameters except for m_5, representing M deficit. The two values of m_5 used change the profile from a surface-based duct to an elevated duct. Results of the forward model runs using both homogeneous and inhomogeneous turbulence models are shown in Figures 4, and 5. Theoretically, only surface-based ducts should cause trapping of propagating waves between the duct height and Earth's surface [*Gerstoft et al.*, 2000], Figure 5 shows that the inhomogeneous turbulence model can produce similar trapping in elevated ducts.

3. Stochastic Forward Model

As previously stated, a PE method [*Tappert*, 1977] is used to calculate the amplitude $U(x,z)$ of propagative EM fields over a grid of ranges x and heights z. The PE method is derived from the parabolic equation [*Levy*, 2000]

$$\frac{\partial U(x,z)}{\partial x} = \left[\frac{jk_0}{2}\left(n^2-1\right) + \frac{j}{2k_0}\frac{\partial^2}{\partial z^2}\right]U(x,z) \tag{13}$$

$$= \left[\frac{jk_0}{2}\left(\langle n(z)\rangle^2 + \tilde{n}(x,z)^2 - 1\right) + \frac{j}{2k_0}\frac{\partial^2}{\partial z^2}\right]U(x,z) \tag{14}$$

$$= [A(x,z) + B(z)]U(x,z) \tag{15}$$

$$A(x,z) = \frac{jk_0}{2}\left[\left\langle n(z)^2\right\rangle + \tilde{n}(x,z)^2 - 1\right]; \quad B(z) = \frac{j}{2k_0}\frac{\partial^2}{\partial z^2} \tag{16}$$

where $k_0 = \omega/c$ is a reference wave number and $j = \sqrt{-1}$. The solution to (16) can be written as

$$U(x+\delta x, z) = U(x,z)\exp\left[\int_x^{x+\delta x}(A+B)\mathrm{d}x\right] \tag{17}$$

$$\approx U(x,z)\exp\left[(A+B)\delta x\right] \tag{18}$$

$$\approx U(x,z)\exp\left[A\delta x\right]\exp\left[B\delta x\right]. \tag{19}$$

Equation (18) assumes A varies slowly with range, while equation (19) assumes A and B commute; however, A and B only commute for n constant in z. Error introduced by the assumptions of equations (18) and (19) is discussed in section 3.2.2. The split performed in equation (19) is the basis of the split step PE method.

The stochastic forward model is an augmented version of the PE forward model denoted as $F\left(\mathbf{m}, C_n^2\right)$, where $\mathbf{m}$ is the refractivity profile parameter vector and C_n^2 is the structure function constant of the observed turbulence which corresponds to the magnitude of $\tilde{n}(z)$. Specification of C_n^2 allows control of the variance of $\tilde{n}(z)$ which is generated inside the model and added to $\langle n(z)\rangle$.

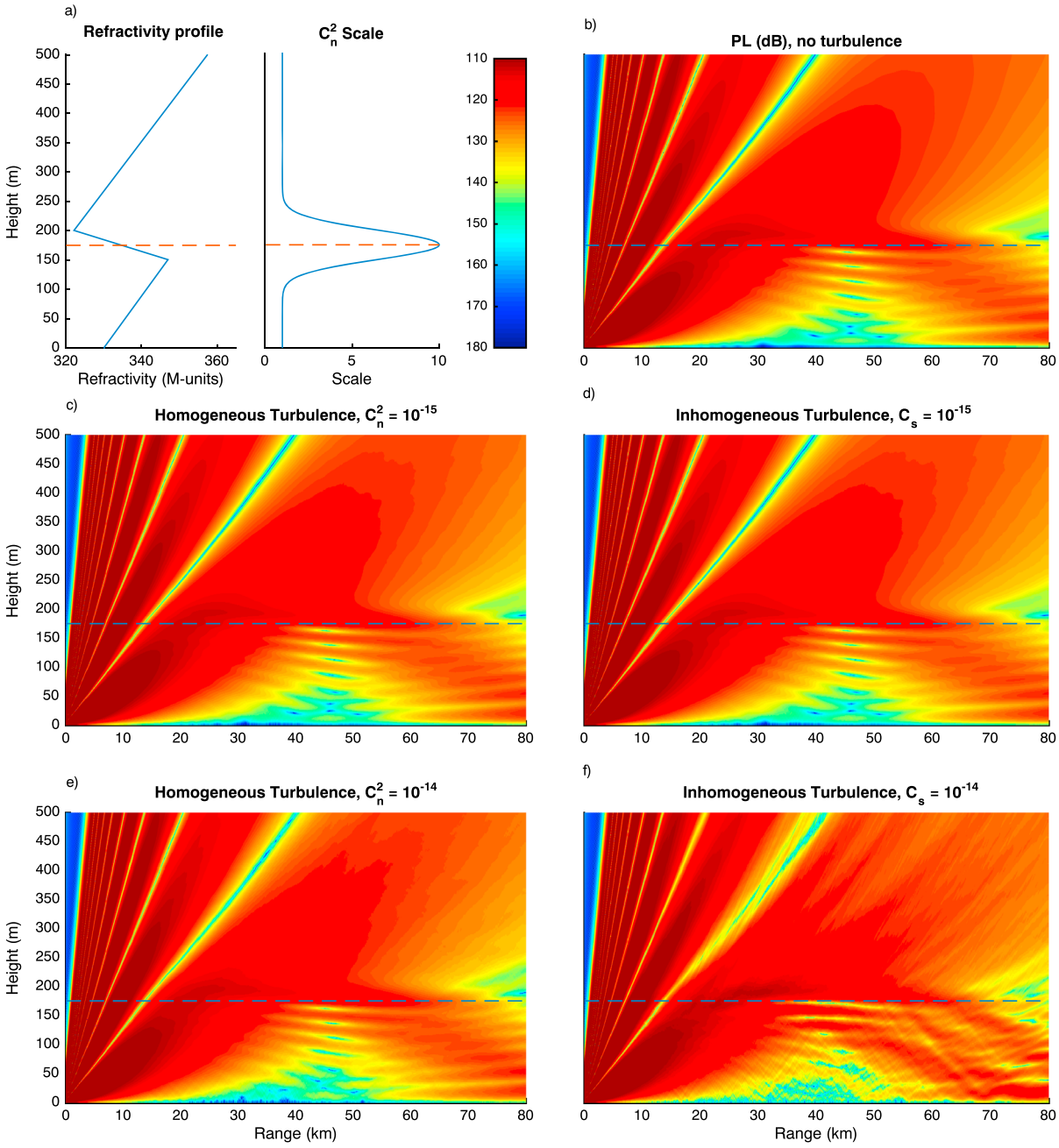

Figure 4. (a) Surface-based duct refractivity profile and C_n^2 profile. (b) Propagation loss (PL) of 1 GHz wave given refractivity and C_n^2 profiles in Figure 4a under no turbulence. PL calculated assuming homogeneous turbulence given (c) $C_n^2 = 10^{-15}$ and (e) 10^{-14}. PL calculated assuming inhomogeneous turbulence given (d) $C_s = 10^{-15}$ and (f) $C_n^2 = 10^{-14}$.

3.1. Parabolic Equations and Simulating Turbulence

The numeric solution to the split step PE method defined in equation (19) is written as

$$U(x+\delta x, z) = \frac{1}{2\pi}\exp[j\kappa\phi(z)]\mathrm{F}^{-1}\left[e^{\mathrm{WAPE}}\mathrm{F}\left[U(x,z)\right]\right] \tag{20}$$

where F[·] represents the Fourier transform (FT), κ is the wave number, WAPE is the standard wide angle PE propagator, and $\exp[j\kappa\phi(z)]$ is known as the transmittance function. The PE method is summarized as follows [*Levy*, 2000]: a Fourier transform of the starting field propagating in the x direction is taken with respect to

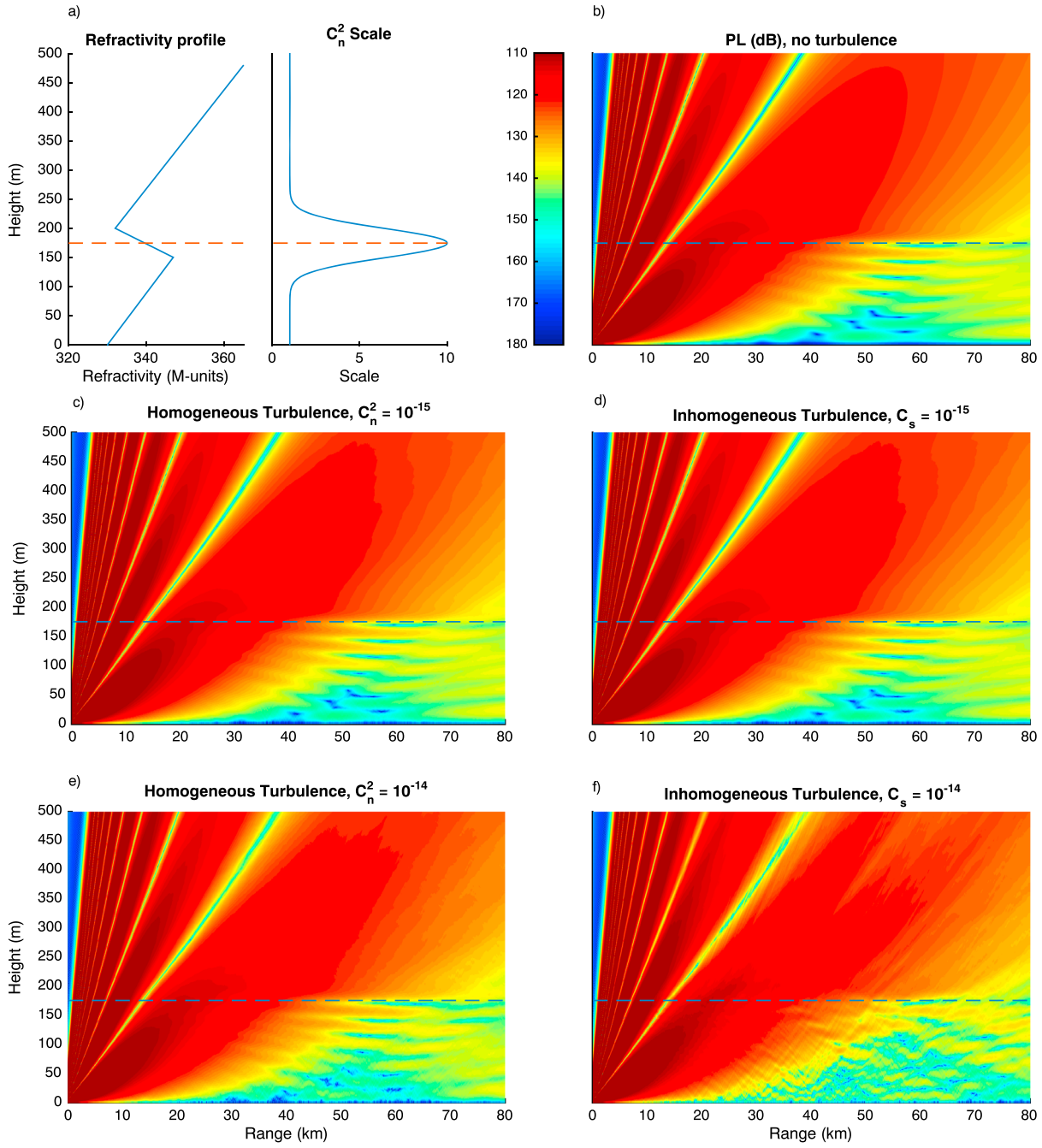

Figure 5. (a) Elevated duct refractivity profile and C_n^2 profile. (b) Propagation loss (PL) of 1 GHz wave given refractivity and C_n^2 profiles in Figure 5a under no turbulence. PL calculated assuming homogeneous turbulence given (c) $C_n^2 = 10^{-15}$ and (e) 10^{-14}. PL calculated assuming inhomogeneous turbulence given (d) $C_s = 10^{-15}$ and (f) $C_n^2 = 10^{-14}$.

z and multiplied by a propagation filter. The inverse transform is then taken and multiplied by a transmittance function which accounts for the change in phase between range x and $x + \delta x$. The PE algorithm marches down the x axis, calculating each successive field amplitude using the previous field amplitude as input. The transmittance function $\phi(z)$ comes from the $e^{A\delta x}$ term in equation (19) and is defined as

$$\phi(z) = \frac{1}{2}\int_x^{x+\delta x} \left[\langle n(x,z)\rangle^2 + \tilde{n}(x,z)^2 - 1\right] \mathrm{d}x + z\delta x/a_e, \tag{21}$$

where a_e is the Earth radius in kilometers and the term $z\delta x/a_e$ has been added to correct for the curvature of the Earth. Knowing the ratio $\tilde{n}/\langle n\rangle \ll 1$ and neglecting second-order terms, we simplify the integral (21) so that only fluctuations over δx are nontrivial

$$\phi(z) = \left[\langle n(z)\rangle^2 - 1 + z/a_e\right]\delta x + \tilde{\phi}(z) \tag{22}$$

$$\tilde{\phi}(z) = \int_x^{x+\delta x} \tilde{n}\left(x', z\right)^2 \mathrm{d}x' \tag{23}$$

where $\tilde{\phi}(z)$ is the randomly fluctuating part of the transmittance function. The transmittance function represents total phase change of the wave over range step δx, so to generate accurate realizations of PL using the PE method, we must know the spectrum of fluctuations integrated over a distance δx, generate realizations of this spectrum using (9), and add them to the transmittance function at every range step. This spectrum is known as the *transverse spectrum*. The transverse spectrum is obtained from the spectrum of refractivity (8) through integration of the corresponding autocorrelation function over range (assuming $\delta x > L_0$) [*Rouseff*, 1992].

$$S_t(\kappa_z) \approx \frac{0.033(2\pi)^2}{\left(\kappa_z^2 + L_0^{-2}\right)^{4/3}} \delta x C_n^2 \pi^{1/2} \frac{\Gamma(4/3)}{\Gamma(11/6)}. \tag{24}$$

Note that this paper assumes the existence of a universal statistical description of small-scale turbulence which may not actually exist [*Frehlich and Sharman*, 2004], [*Fabbro and Féral*, 2012]. If later research leads to a more accurate method of modeling realizations of turbulence, it may be substituted into this work without changing the inversion algorithm.

For notational simplicity we will continue to denote fluctuations in refractivity generated from the transverse spectrum in (24) as $\tilde{n}(z)$. We simplify our algorithm by generating independent realizations of $\tilde{n}(z)$ at each range step of the PE, an assumption that will be explored in the next section.

3.2. Sources of Error in the PE

Here the sources of error in the forward model $F\left(\mathbf{m}, C_n^2\right)$ are explored. As mentioned in the previous section, there are several approximations made by the PE method and its modification for the inclusion of turbulence. Our goal is to identify each source of error and quantify their magnitudes. The sources of error include limitations in range and height step size by the turbulence model, approximations made in the derivation of the PE method, error in the turbulence model, and effects of polarization which are not considered by the model.

3.2.1. Height and Range Resolution

To generate independent realizations of refractivity fluctuations in height between ranges x and $x + \delta x$, we have assumed that the range step δx is large enough that fluctuations between range steps are independent. The integral length scale introduced in section 2.2.3 is the integral of the longitudinal correlation between two points distance r apart.

$$L_0 = \int_0^\infty R(r)\mathrm{d}r \tag{25}$$

where $R(r)$ is the autocorrelation function of refractivity as a function of distance r between the points. Equation (25) reveals that the integral length scale is a measure of the minimum distance between uncorrelated points; therefore, so long as $L_0 < \delta x$, simulated turbulence will be independent between realizations of $\tilde{n}(z)$ at range steps δx apart. Recall the model spectrum in equation (8) uses L_0 as a parameter. Here $L_0 = 10$ m was used. This value was also used in a similar study on turbulence modeling [*Rouseff*, 1991]. Experimental measurements of the integral length scales of wind velocity and temperature find values between 2 and 20 m [*Wang et al.*, 1992]. We have assumed that the integral length scale of refractivity is similar to that of wind velocity and temperature, a reasonable assumption considering refractivity is a function of temperature.

The range step size of our forward model is primarily a function of signal frequency f_c [*Barrios*, 2008]

$$\delta x = \frac{\pi c}{f_c \sin^2\left(\theta_{\max}\right)} \tag{26}$$

where c is the speed of light in a vacuum and θ_{max} is the maximum propagation angle of the propagating wave and has been set to 7.45° for all inversions to emulate a directional antenna. According to (26), EM wave frequencies that result in range steps larger than the integral length scale are acceptable. Plugging $L_0 = 10$ m and $\theta_{max} = 7.45°$ into equation (26) we get a maximum acceptable simulated wave frequency of $f_c = 5.61$ Gz.

Now we turn to the height step size, which we will denote as δz. The maximum height step is $\delta z = L_0$ because for larger step sizes fluctuations in turbulence are uncorrelated, defeating the purpose of modeling turbulence from a spectrum. The minimum height step is $\delta z = l_0$ because the von Karman spectrum is not accurate for wave numbers larger than l_0^{-1}. The value of δz in the PE model is selected according to

$$\delta z = \frac{c}{2f_c \sin\left(\theta_{max}\right)} \tag{27}$$

Once calculated, the value of δz is rounded down such that the number of height steps between the ocean surface and the maximum simulated height is a power of 2. The maximum height is an input to the forward model; each inversion in this paper uses max height equal to 1 km and results in 1024 evenly spaced height steps between 0 and 1000 m. Experimental values of l_0 are on the scale of 10^{-3} to 10^{-2} m.

Note that a model spectrum typically used to describe turbulence in wind velocity is being used to model that of refractivity. This may be a source of error because refractivity is a function of T, P, and e, (see equation (3)) all of which have some relation to wind velocity but are not identical. A wind velocity spectrum was used as the model spectrum because wind velocity is an area of significantly more focus in the literature than T, P, and e.

3.2.2. Error From Assumptions in the PE Method

Two assumptions are made in the Parabolic equation, equations (17)–(19). The first assumption is that the refractivity profile varies slowly in range, and the second assumption is that terms A and B commute. While our model assumes range independence of the refractivity profile, stochastic variations from $\tilde{n}$ cause changes in refractivity between range steps. Additionally, A and B do not commute because B is a differential operator and n is expected to change in z. An evaluation of the error caused by ignoring the commutator term on a range-dependent PE is performed in *Craig and Levy* [1991, equation 20], where it is found that

$$E = \delta x \left[jk_0 n \frac{\partial \tilde{n}}{\partial x} U(x,z) + n \frac{\partial n}{\partial z} \frac{\partial U}{\partial z} + \frac{nU}{2} \frac{\partial^2 n}{\partial z^2} + \frac{U}{2} \left(\frac{\partial n}{\partial z} \right)^2 \right] + \mathrm{O}\left[(\delta x)^2\right] \tag{28}$$

which depends on range step δx, wave frequency, and refractive index gradient in both x and z directions and is guaranteed to increase on the order of δx^2. Simulations performed here use range step sizes on the order of 100 m, at 1 GHz, so the commutator error may become a significant source of error at this range. It is possible to reduce this error by using an alternate splitting of the PE, which may be implemented in future work.

3.2.3. Errors in the Turbulence Model

The proposed forward model, $F\left(\mathbf{m}, C_n^2\right)$ handles turbulence and refractivity separately, by inserting randomly generated fluctuations described by C_n^2 to an environment with an independent refractivity profile parameterized by $\mathbf{m}$. However, there is some evidence of a connection between C_n^2 and $\mathbf{m}$, especially in an inversion layer, through the dissipation rate of turbulence [*Peltier and Wyngaard*, 1995]. Turbulence is a dissipative mechanism for kinetic energy cascading from large to small scales. The input for this energy is primarily wind shear, which can influence the temperature gradient in the z direction, and by proxy the refractivity gradient within a duct. Thus, the simplified model used here does not fully reflect the interactions between turbulence and refractivity, which may be a future focus.

3.2.4. Error From Polarization

The PE method is a forward-scatter approximation to the Helmholtz wave equation for either the electric field of a horizontally polarized wave or the magnetic field of a vertically polarized wave [*Levy*, 2000]. Wave polarization impacts the solution of the PE at the boundaries, here between ocean and air. Our PE forward model solves only for the electric field associated with a horizontally polarized wave and assumes a Dirichlet boundary condition on the ocean surface [*Dockery and Kuttler*, 1996].This implies the ocean is a perfectly conducting surface. Because a rough ocean will not perfectly reflect all energy, it might be better modeled with a nonzero impedance [*Dockery and Kuttler*, 1996], [*Rosenberg*, 1999].

4. Bayesian Inversion

We now infer $\langle n(z) \rangle$ given PL measurement vector $\mathbf{d}$ under a Bayesian framework. The unknown variables are the entries of the $\mathbf{m}$ vector, with unknown posterior probability distribution (pdf). The joint pdf of $\mathbf{m}$ is the probability of $\mathbf{m}$ given the N_d dimensional data $\mathbf{d}$, $\mathrm{p}(\mathbf{m}|\mathbf{d})$ is known as the posterior pdf. The $\mathbf{m}$ with the highest probability is the maximum a posteriori (MAP) solution. Using Bayes rule, we obtain the posterior pdf

$$\mathrm{p}(\mathbf{m}|\mathbf{d}) = \frac{\mathrm{p}(\mathbf{d}|\mathbf{m})\mathrm{p}(\mathbf{m})}{\mathrm{p}(\mathbf{d})} \tag{29}$$

It is clear from (29) that the posterior pdf depends on three terms, $\mathrm{p}(\mathbf{d}|\mathbf{m})$, $p(\mathbf{m})$, and $\mathrm{p}(\mathbf{d})$. Our goal is to find an expression for each distribution.

Though knowledge of the prior on $\mathbf{m}$ may be attainable, we assume that it has a uniform distribution. If some knowledge of the refractivity profile later becomes available through measurement or some statistical means, it can be utilized by this framework. The distribution $\mathrm{p}(\mathbf{d})$ is known as the evidence and is given as

$$\mathrm{p}(\mathbf{d}) = \int_m \mathrm{p}(\mathbf{d}|\mathbf{m})\mathrm{p}(\mathbf{m})\mathrm{d}\mathbf{m}. \tag{30}$$

The evidence is not of importance here. The term reduces to a constant, serving as a normalization factor to ensure $\mathrm{p}(\mathbf{m}|\mathbf{d})$ integrates to unity. Neglecting the evidence gives

$$\mathrm{p}(\mathbf{m}|\mathbf{d}) \propto \mathrm{p}(\mathbf{d}|\mathbf{m})\mathrm{p}(\mathbf{m}), \tag{31}$$

where $\mathrm{p}(\mathbf{d}|\mathbf{m})$ is the likelihood function.

4.1. Likelihood Function

To create a likelihood function, we model the measurement vector $\mathbf{d}$ as

$$\mathbf{d} = \boldsymbol{g}_K(\mathbf{m}) + \boldsymbol{n} \tag{32}$$

where $\boldsymbol{n}$ is a noise vector of measurement and model error and $\boldsymbol{g}_K(\mathbf{m})$ is the average of K realizations of $F\left(\mathbf{m}, C_n^2\right)$ to reduce stochastic fluctuations in the forward model.

$$\boldsymbol{g}_K(\mathbf{m}) = \frac{1}{K}\sum_{k=1}^{K} F\left(\mathbf{m}, C_n^2\right)_k . \tag{33}$$

We model $\mathbf{n}$ as a Gaussian noise vector

$$\boldsymbol{n} \in N\left(0, \boldsymbol{\Sigma}_d\right) \tag{34}$$

where $\boldsymbol{\Sigma}_d$ is the true covariance matrix of $\mathbf{d}$ which we approximate with $\mathbf{C}_d$ the maximum likelihood estimate of K runs of $\mathbf{f}\left(\mathbf{m}, C_n^2\right)$

Because $\boldsymbol{n}$ is Gaussian, we use the standard zero mean Gaussian likelihood function to measure the likelihood of $\mathbf{d}$ coming from refractivity profile $\mathbf{m}$.

$$\mathrm{p}(\mathbf{d} \mid \mathbf{m}) = \frac{1}{\sqrt{(2\pi)^{N_d}|\mathbf{C}_d|}} \exp\left(-\frac{\left(\mathbf{d} - \boldsymbol{g}_K(\mathbf{m})\right)^T \mathbf{C}_d^{-1}\left(\mathbf{d} - \boldsymbol{g}_K(\mathbf{m})\right)}{2}\right), \tag{35}$$

where N_d is the length of $\mathbf{d}$. Note that $\mathbf{C}_d$ might be singular because of computer precision errors caused by extremely small variance at short ranges. Adding a small diagonal load is recommended to prevent computation errors. Because the likelihood function is strictly monotonic and the terms outside the exponential do not contain input $\mathbf{d}$, we simplify equation (35) to an objective function

$$\phi = \left(\mathbf{d} - \boldsymbol{g}_K(\mathbf{m})\right)^T \mathbf{C}_d^{-1}\left(\mathbf{d} - \boldsymbol{g}_K(\mathbf{m})\right), \tag{36}$$

which must be minimized.

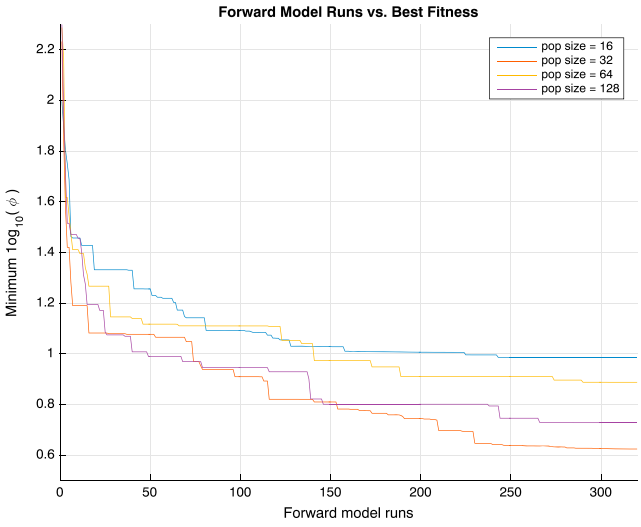

Figure 6. Average convergence of GA with population sizes [16, 32, 64, 128] for measurement **d** taken from elevated duct refractivity environment with $C_n^2 = 10^{-15}$.

4.2. Genetic Algorithm

From (36) we have an objective function for evaluating the MAP estimate of **m**. To uncover the MAP estimate $\hat{\mathbf{m}}$, we run a genetic algorithm (GA) over the continuous space of possible **m**, choosing realistic upper and lower bounds on the parameters of the M-profile. The crossover rate of the GA was set to 0.9 for all inversions, though the parameters of the GA may be adjusted to assure more or less accurate results at the cost of computation time. A plot of GA convergence per forward model run for various population sizes is shown in Figure 6 computed using identical observation vectors **d**. Note that our convergence plot is evaluating the objective function in equation (36). Each line in Figure 6 represents the average of five inversion runs to account for randomness. It appears that a population size of 32 has the best convergence properties. All inversions performed in this paper were performed with a population size of 32 over 10 generations.

4.3. The "No Duct" Case

In practice it is often the case that no duct is present in the refractivity profile being evaluated; however, this scenario is represented by only a few of the possible **m** vectors. Given the parameterized M-profile in section 2.1, a standard atmosphere case where no duct is present is described only when m_1, m_4, and m_5 are zero, and $m_2 \approx .113$ M-units. Given this circumstance, use of a GA becomes problematic for two reasons. First, the GA is designed to sample sparsely over the search space and navigate to a maximum point stochastically. If the no duct case is not sampled by the algorithm (which is likely), it will lead to misidentification of a no duct event as a ducting event almost certainly. Next, in the scenario where the no duct **m** is evaluated, another **m** can be scored as slightly more likely than the no duct case due to measurement noise.

Introduction of a prior probability on the space of **m** vectors is needed to remedy the shortcomings of the optimization. Use of a prior requires slight modifications in (31) to account for the prior probability of no duct.

Using a uniform prior over the set of all ducting events and a corresponding prior for the no duct case is a simple method that may be used with good success. The set of **m** vectors, $\mathbf{M}_{\text{nd}}$, which denote no duct are described by $\mathbf{m} \in [0, .13, m_3, 0, 0]$. All other **m** vectors denote some type of duct. Using this knowledge we have

$$\text{p}(\mathbf{m} \mid \mathbf{d}) \propto \text{p}(\mathbf{d} \mid \mathbf{m})\text{p}(\text{duct}), \quad \mathbf{m} \in \mathbf{M}_{\text{nd}} \tag{37}$$

$$\text{p}(\mathbf{m} \mid \mathbf{d}) \propto \text{p}(\mathbf{d} \mid \mathbf{m})\text{p}(\text{no duct}), \quad \mathbf{m} \notin \mathbf{M}_{\text{nd}}. \tag{38}$$

The probability of the no duct case should reasonably reflect the frequency of ducting phenomenon in the region where **d** was measured and can be obtained from a climatology database [*Yardim et al.*, 2009] or from a numerical weather prediction algorithm [*Karimian et al.*, 2012]. To avoid problems incurred when the genetic algorithm does not evaluate the probability of a no duct scenario, the likelihood of the no duct **m** vector should be evaluated prior to running the algorithm and compared to the results.

4.4. Inversion Algorithm

The inversion algorithm is explained in detail below:

1. Measure both **d** and average C_n^2.
2. Evaluate equation (38) using **d**, and $\mathbf{C}_d$, $\boldsymbol{g}_K(\mathbf{m})$ simulated with any $\mathbf{m} \in \mathbf{M}_{\text{nd}}$. The resulting probability is the probability of a no duct scenario.

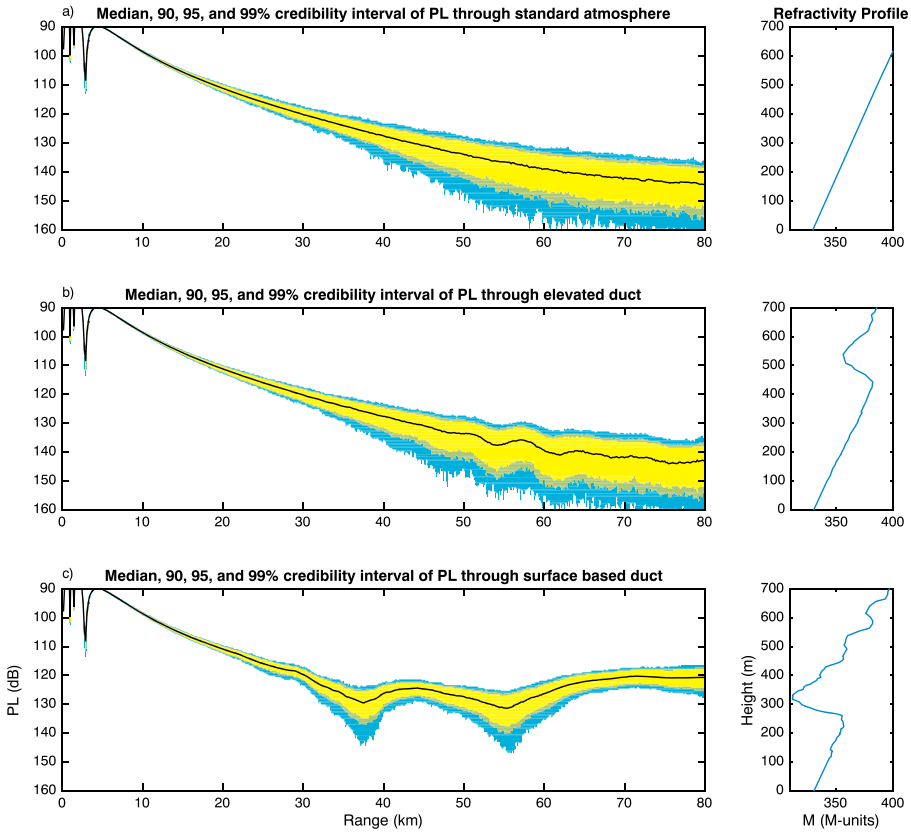

Figure 7. Median and 90, 95, and 99% credibility interval of propagation loss (PL) for 300 MHz wave at 20 m propagating through (a) standard atmosphere, (b) elevated duct, and (c) surface-based duct with structure function constant $C_n^2 = 10^{-14}$. Generated from 500 Monte Carlo trials assuming homogeneous turbulence.

3. Make an initial guess $\mathbf{m}_0$. Generate the corresponding $\mathbf{C}_{d_0}$ using N Monte Carlo trials of $F\left(\mathbf{m}_0, C_n^2\right)$.
4. Run the GA. The output is $\mathbf{m}_1$.
5. Generate $\mathbf{C}_{d_1}$, rerun the GA using $\mathbf{C}_{d_1}$.
6. Repeat N times
7. Evaluate (37) with input $\hat{\mathbf{m}}$ and (38) using $\mathbf{m} \in \mathbf{M}_{\text{nd}}$. The $\mathbf{m}$ with greatest probability parameterizes the estimated refractivity.

Step 2 is evaluating the probability of no duct and can be discarded if there is no prior information about the environment being simulated. Step 3 asks for a user input, $\mathbf{m}_0$, which is used as an initial guess at the duct being estimated. If nothing is known about the duct, then the user may as well use the standard atmosphere profile from the previous step. This item is important because calculation of the covariance $\mathbf{C}_d$ is the most computationally expensive part of the algorithm. Precalculation of $\mathbf{C}_d$ speeds the inversion up considerably but requires that the algorithm is iterative. Steps 4 through 6 are the main algorithm. An optimal solution is found by the GA using the suboptimal $\mathbf{C}_d$ from the initial guess, the GA outputs the highest fitness solution $\mathbf{m}_{\text{opt}}$ and calculates the corresponding $\mathbf{C}_{d_{\text{opt}}}$. The process then repeats until the algorithm has run a set number of times. The final step compares the likelihood of the solution $\hat{\mathbf{m}}$ with the probability of the standard atmosphere (taking into account the prior likelihood of a standard atmosphere).

5. Inversion Results

Figure 7 shows the 90, 95, and 99% credibility intervals of the pdf of PL through standard atmosphere, elevated duct, and surface-based duct refractivity profiles estimated from 500 Monte Carlo trials under homogeneous turbulence generated by (9) and (10) and spectrum described by (24) . From Figure 7 we see that when simulating homogeneous turbulence, the distribution of PL through standard atmosphere and elevated duct

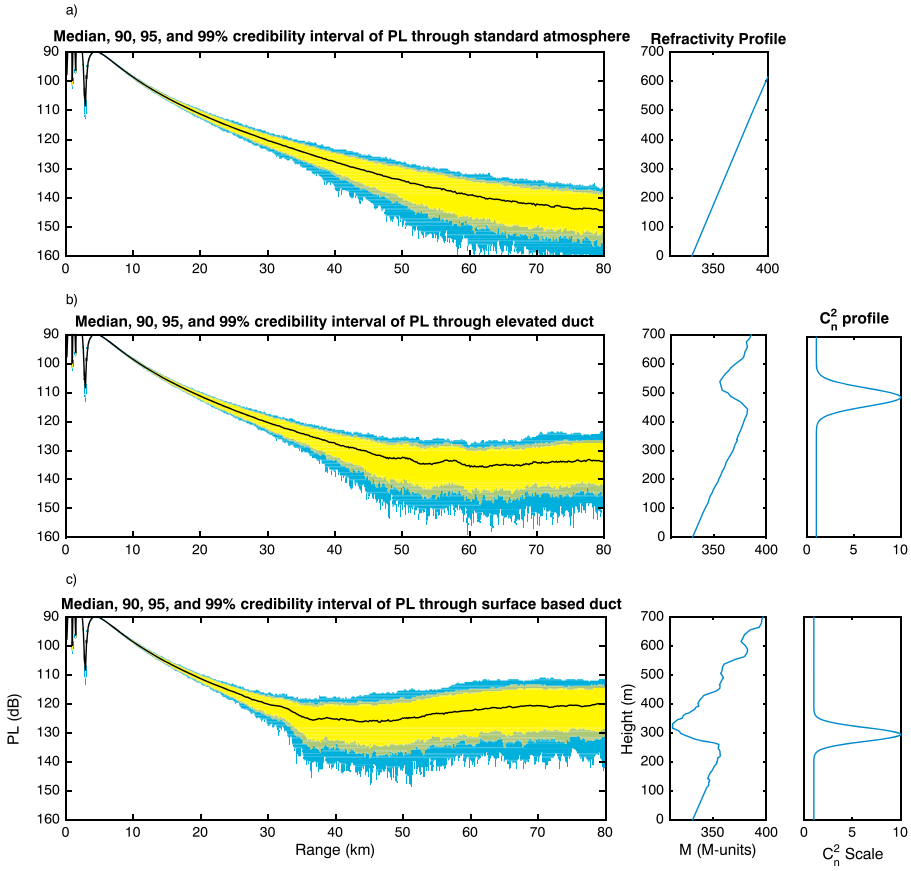

Figure 8. Median and 90, 95, and 99% credibility interval of propagation loss (PL) for 300 MHz wave at 20 m propagating through (a) standard atmosphere, (b) elevated duct, and (c) surface-based duct with structure function constant $C_n^2 = 10^{-14}$. Generated from 500 Monte Carlo trials assuming inhomogeneous turbulence.

refractivity profiles is nearly identical, while surface-based ducts alter the distribution of PL significantly. Accordingly, we expect our inversion algorithm should estimate surface-based ducting profiles well but be unable to distinguish elevated ducts from standard atmosphere refractivity profiles.

Figure 8 shows the same distributions generated with $C_n^2(z)$ described by (12) with $K = 9$. For the elevated duct profile we estimated $m_3 = 443$ m, $m_4 = 95$ m and for the surface-based duct $m_3 = 260$ m, $m_4 = 70$ m. $C_n^2(z)$ remains unchanged for the standard atmosphere profile because there is no inversion layer where turbulence is expected to increase. Under this scheme both elevated and surface-based ducts produce unique distributions and therefore should allow for inversion. A key observation from Figures 7b and 8b is how the height-dependent C_n^2, when modeled as having an increase at the inversion (section 2.3), impacts beyond-line-of-sight (BLOS) propagation for the elevated duct case considered. In Figure 7b the median propagation loss over the region from 60 to 80 km is 142 dB over 500 realizations. In Figure 8b (height-dependent), the value is 135 dB. This suggests that failing to account for the C_n^2 increase at the inversion can negatively bias propagation estimates in the BLOS region. Note that this is consistent with the differences between with and without height dependence show in Figure 5.

Figure 9 shows the covariance matrix, $\mathbf{C}_d$, of PL of a wave propagating through a surface-based duct under both homogeneous and inhomogeneous turbulence. The covariance matrices were sampled from 500 runs of the forward model using the true refractive environment. Information conveyed in these covariance matrices is absent from the inversion algorithm when assuming $\mathbf{C}_d = \alpha \mathbf{I}$.

The parameters of the forward model for the refractivity inversion were chosen such that the propagating wave would be trapped between any existing ducts and the ocean surface. If the wave was to propagate at too steep an angle, it would not be trapped in the duct and we might as well be working with a

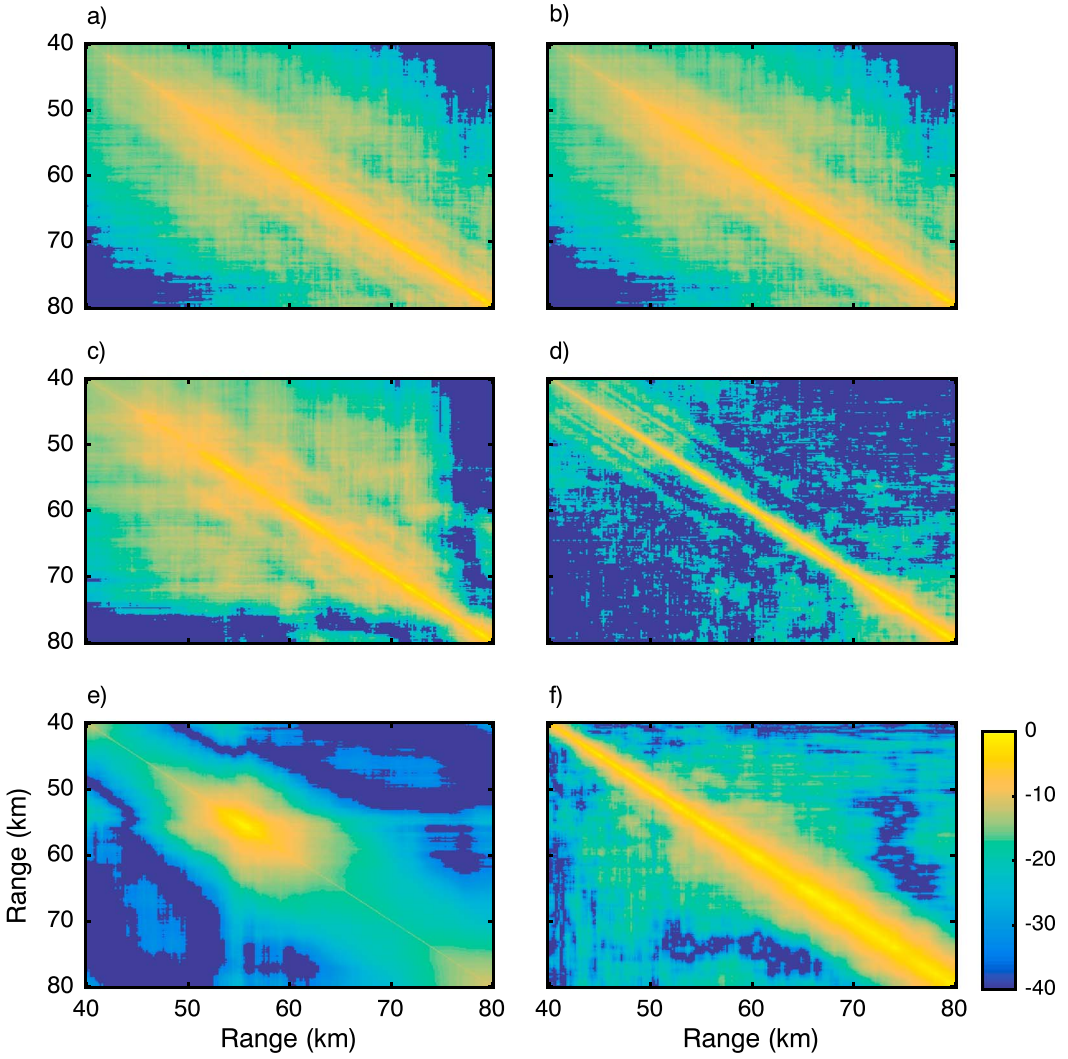

Figure 9. Estimated covariance matrix (in dB) of propagation loss at 20 m height through (a and b) standard atmosphere, (c and d) VOCAR elevated duct, and (e and f) VOCAR surface-based duct. Homogeneous turbulence model used in Figures 9a, 9c, and 9e. Inhomogeneous turbulence used in Figures 9b, 9d, and 9f. Estimates made using (500) forward model runs of propagation loss using $C_n^2 = 10^{-13}$.

standard atmosphere. Outside the possibility that the transmitted wave is not trapped by an existing duct, the transmitter height and propagation angle of the wave should not impact inversion accuracy because the algorithm works by evaluating the first- and second-order statistics of the specific wave being modeled. The same can be said for the height at which PL is measured.

All figures and inversions were performed using PL at constant 20 m height (from the ocean surface) from a transmitter at 10 m transmitting a 300 MHz wave over an 80 km range with vertical beam width of 0.209 radians. The transmitter was pointed horizontally such that the wave propagated normal to the line formed between the transmitter and the ocean surface. The genetic algorithm used in the inversion ran over 10 generations with a population size of 32 and a crossover fraction of 0.1. Each inversion consisted of 60 GA runs. Inversions were run comparing 60 iterations of the algorithm in section 4.4 and 60 inversions where $\mathbf{C}_d = \sigma^2\mathbf{I}$. The two inversion strategies are compared in Figures 10 and 11.

The initial measurement vector, **d**, was simulated using the forward model propagating through the true refractivity profile over an 80 km range. The simulated **d** vector was 1234 points long, with a step size of 64 m. Two refractive environments were estimated. First, a surface-based duct from the VOCAR 1993 experiment [*Paulus*, 1994] with homogeneous turbulence generated by (9) and (10) and spectrum described by (24).

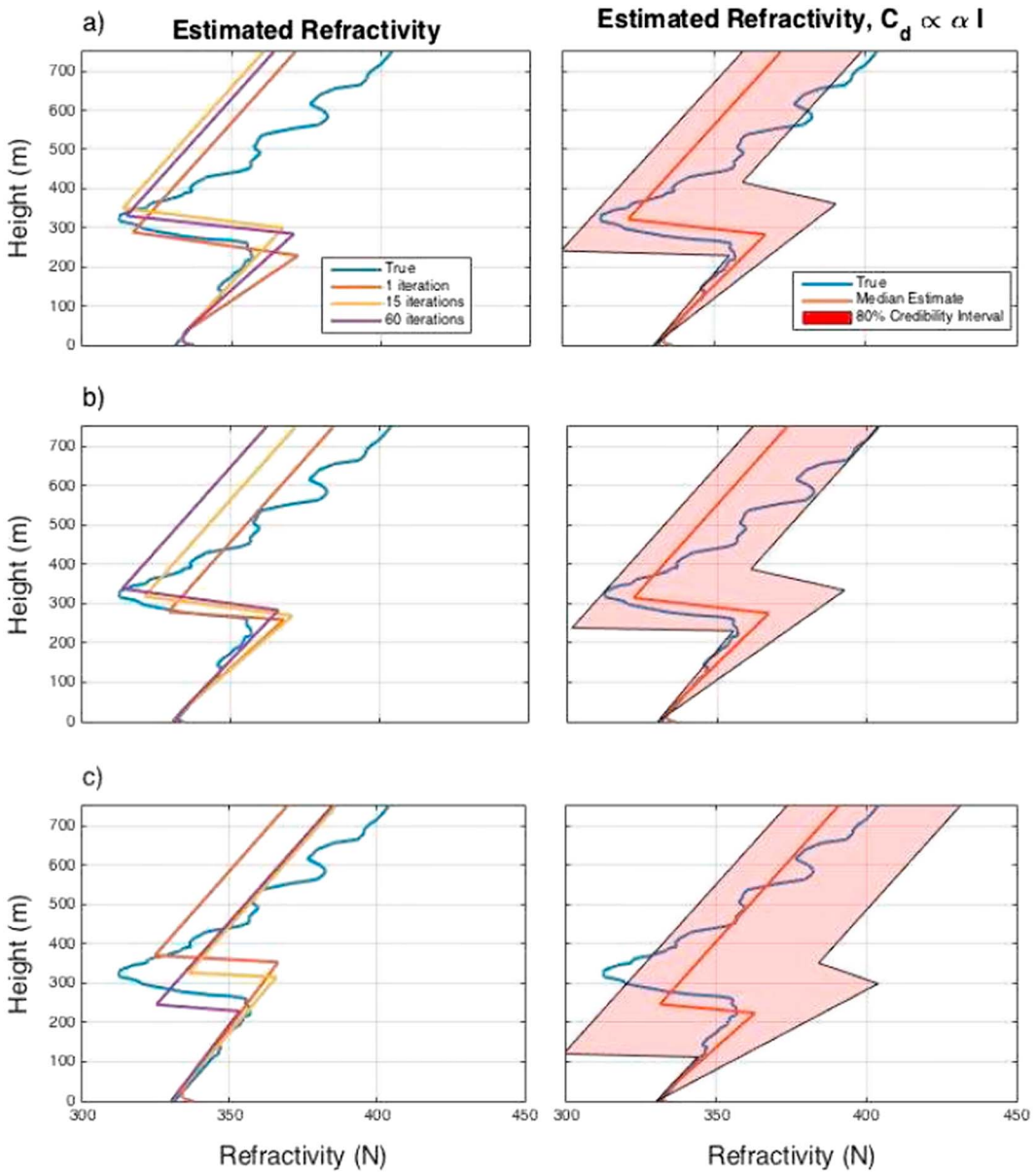

Figure 10. Estimated refractivity for surface-based duct measured in VOCAR 1993 experiment assuming homogeneous turbulence, (a) $C_n^2 = 10^{-17}$, (b) $C_s = 10^{-15}$, and (c) $C_s = 10^{-13}$. (left column) Inversions performed using Monte Carlo estimate of $\mathbf{C}_d$ (Figures 10a–10c); (right column) $\mathbf{C}_d$ assumed proportional to $\alpha\mathbf{I}$.

Next, an elevated duct from the VOCAR 1993 experiment with inhomogeneous turbulence simulated using (12). An inhomogeneous turbulence model is used for inversions on the elevated duct because Figures 7 and 9 show that under a homogeneous turbulence model, the elevated duct will be nearly indistinguishable from a standard atmosphere profile.

Figure 10 has two columns. The left column shows the inversion result after 1, 15, and 60 iterations of the algorithm in section 4.4. The right column shows the median and 80% credibility intervals of the estimated refractivity profiles after 60 independent inversions. Both columns show inversions performed on a surface-based duct over a range of C_n^2 values assuming homogeneous turbulence. Figure 10 show that the iterative algorithm hits an accurate solution after 15 iterations and does not change significantly in subsequent iterations. The Monte Carlo trials which ignore $\mathbf{C}_d$ produce an accurate median solution but have a wide credibility interval, indicating that individual solutions may not be very accurate. Both inversion methods appear to lose accuracy as C_n^2 increases. Figure 11 is consistent with Figure 10 in these regard.

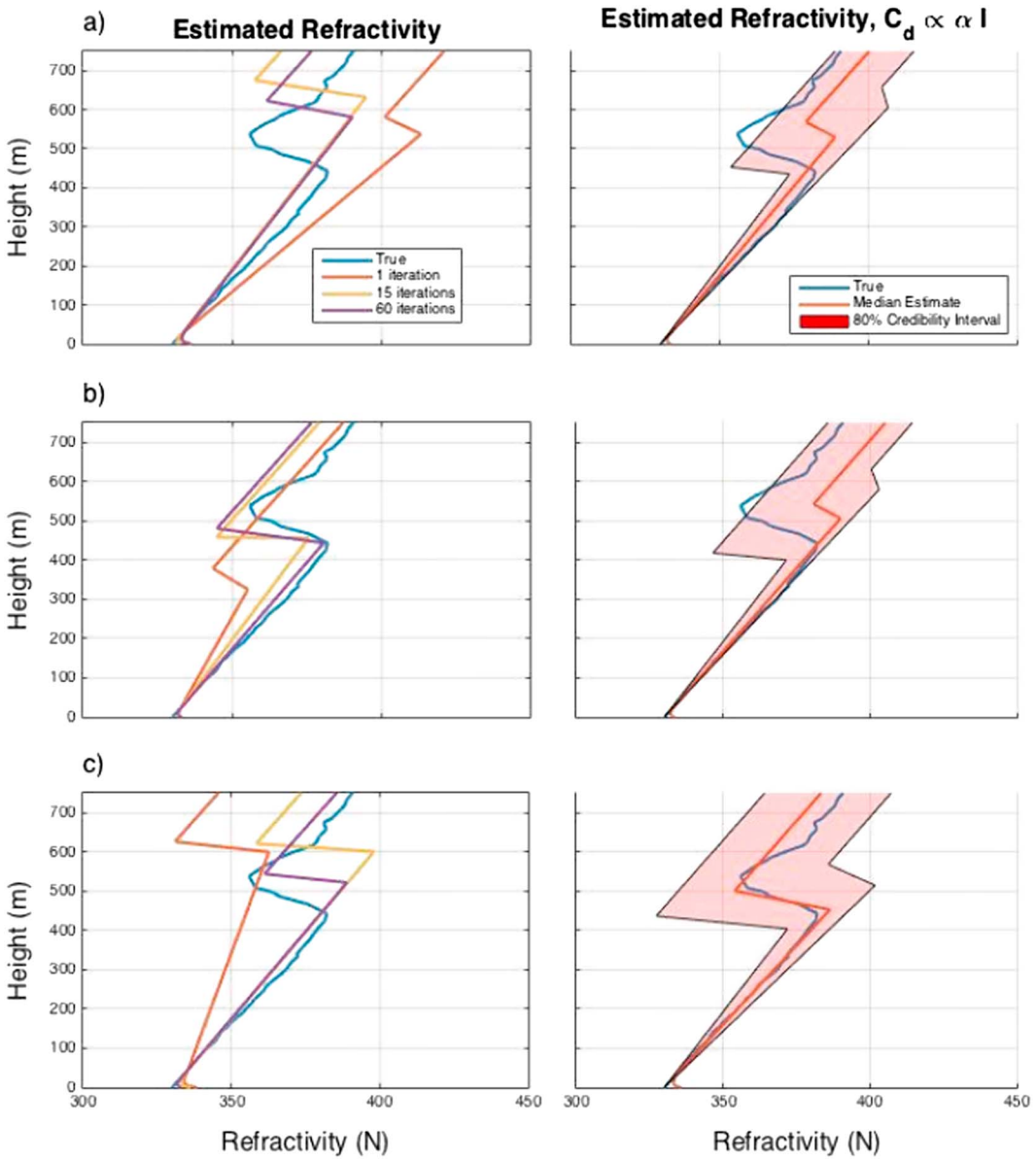

Figure 11. Estimated refractivity for elevated duct measured in VOCAR 1993 experiment assuming inhomogeneous turbulence, (a) $C_n^2 = 10^{-17}$, (b) $C_s = 10^{-15}$, and (c) $C_s = 10^{-13}$. (left column) Inversions performed using Monte Carlo estimate of $\mathbf{C}_d$; (right column) $\mathbf{C}_d$ assumed proportional to $\alpha\mathbf{I}$.

6. Conclusions

An inversion scheme was proposed for estimation of atmospheric refractivity given measured PL **d** at constant height in presence of turbulence. The mean and covariance of error in PL measurements was estimated using Monte Carlo trials and used to evaluate a likelihood function for parameterized refractivity profiles. A genetic algorithm was then applied to search over the parameter space to find the MAP refractivity profile, which was compared in accuracy to refractivity profiles found using a likelihood function assuming spatially uncorrelated errors ($\mathbf{C}_d \propto \mathbf{I}$).

Two models of turbulence were used to simulate refractivity fluctuations, a homogeneous model where C_n^2 was constant, and a more realistic inhomogeneous model where C_n^2 reached a distinct peak at the inversion layer. Inversion results showed that the inhomogeneous turbulence profile caused elevated ducts to produce trapping below the inversion layer, an effect which is limited to surface-based ducts in nonturbulent environments. Additionally, despite the increased refractivity fluctuations introduced by the inhomogeneous

turbulence, inversion under such a scheme produced accurate estimates of the parameters of an elevated duct which otherwise would have been mistaken for a standard atmosphere profile. The results suggest that turbulence can significantly alter PL of waves traveling through atmospheric ducts by increasing the strength of existing ducts.

For inversions, use of Monte Carlo trials to estimate covariance of PL appeared to increase the accuracy of inversions performed on ducts with ambiguous mean PL patterns. Analysis of PL from standard atmosphere and elevated and surface-based duct refractivity profiles showed that homogeneous and inhomogeneous turbulence models produced different PL distributions for the same refractivity profiles. Turbulence can have a significant impact on the distribution of PL, so accuracy of refractivity inversion is limited by our ability to correctly model turbulence.

Acknowledgments
This paper was sponsored by funding from the Office of Naval Research (ONR) grant N00014-15-1-2490 and N0001416WX00973. The authors send special thanks to Amalia Barrios who provided the original split step parabolic equation function which was modified to include turbulent fluctuations. All requests for MATLAB scripts and data should be made to Mark Wagner at m2wagner@eng.ucsd.edu.

References

Barrios, A. E. (1992), Parabolic equation modeling in horizontally inhomogeneous environments, *IEEE Trans. Antennas Propag.*, *40*(7), 791–797, doi:10.1109/8.155744.

Barrios, A. E. (2008), Modeling surface layer turbulence effects at microwave frequencies. paper presented at 2008 IEEE Radar Conference, pp. 1–6., IEEE, 26–30 May.

Chamecki, M., and N. Dias (2004), The local isotropy hypothesis and the turbulent kinetic energy dissipation rate in the atmospheric surface layer, *Q. J. R. Meteorol. Soc.*, *130*(603), 2733–2752, doi:10.1256/qj.03.155.

Craig, K. H., and M. F. Levy (1991), Parabolic equation modelling of the effects of multipath and ducting on radar systems, *IEE Proceedings F - Radar and Signal Processing*, *138*(2), 153–162, doi:10.1049/ip-f-2.1991.0021.

Dockery, D., and J. R. Kuttler (1996), An improved impedance-boundary algorithm for fourier split-step solutions of the parabolic wave equation, *IEEE Trans. Antennas Propag.*, *44*(12), 1592–1599.

Douvenot, R., V. Fabbro, P. Gerstoft, C. Bourlier, and J. Saillard (2008), A duct mapping method using least squares support vector machines, *Radio Sci.*, *43*, RS6005, doi:10.1029/2008RS003842.

Fabbro, V., and L. Féral (2012), Comparison of 2D and 3D electromagnetic approaches to predict tropospheric turbulence effects in clear sky conditions, *IEEE Trans. Antennas Propag.*, *60*(9), 4398–4407, doi:10.1109/TAP.2012.2207070.

Frehlich, R., and R. Sharman (2004), Estimates of turbulence from numerical weather prediction model output with applications to turbulence diagnosis and data assimilation, *Mon. Weather Rev.*, *132*(10), 2308–2324, doi:10.1175/1520-0493.

Gerstoft, P., D. F. Gingras, L. T. Rogers, and W. S. Hodgkiss (2000), Estimation of radio refractivity structure using matched-field array processing, *IEEE Trans. Antennas Propag.*, *48*(3), 345–356, doi:10.1109/8.841895.

Gerstoft, P., L. T. Rogers, J. L. Krolik, and W. S. Hodgkiss (2003), Inversion for refractivity parameters from radar sea clutter, *Radio Sci.*, *38*(3), 8053, doi:10.1029/2002RS002640.

Gilbert, K. E., X. Di, S. Khanna, M. J. Otte, and J. C. Wyngaard (1999), Electromagnetic wave propagation through simulated atmospheric refractivity fields, *Radio Sci.*, *34*(6), 1413–1435, doi:10.1029/1999RS900078.

Ishimaru, A. (1978), *Wave Propagation and Scattering in Random Media*, vol. 2, Acad. Press, New York.

Karimian, A., C. Yardim, P. Gerstoft, W. S. Hodgkiss, and A. E. Barrios (2011), Refractivity estimation from sea clutter: An invited review, *Radio Sci.*, *46*, RS6013, doi:10.1029/2011RS004818.

Karimian, A., C. Yardim, T. Haack, P. Gerstoft, W. S. Hodgkiss, and L. T. Rogers (2012), Towards assimilation of atmospheric surface layer using weather prediction and radar clutter observations, *J. Appl. Meteorol.*, *52*, 2345–2355.

Kolmogorov, A. N. (1941), The local structure of turbulence in incompressible viscous fluid for very large Reynolds numbers, *Dokl. Akad. Nauk SSSR*, *30*, 299–303.

Lentini, N., and E. Hackett (2015), Global sensitivity of parabolic equation radar wave propagation simulation to sea state and atmospheric refractivity structure, *Radio Sci.*, *50*, 1027–1049, doi:10.1002/2015RS005742.

Levy, M. (2000), *Parabolic Equation Methods for Electromagnetic Wave Propagation*, The Inst. of Electr. Eng., IET, U. K.

Paulus, R. A. (1994), VOCAR: An experiment in variability of coastal atmospheric refractivity, in *Geoscience and Remote Sensing Symposium, 1994. IGARSS '94. Surface and Atmospheric Remote Sensing: Technologies, Data Analysis and Interpretation., International*, vol. 1, pp. 386–388, doi:10.1109/IGARSS.1994.399132.

Peltier, L., and J. Wyngaard (1995), Structure-function parameters in the convective boundary layer from large-eddy simulation, *J. Atmos. Sci.*, *52*(21), 3641–3660.

Percival, D. B. (1993), Simulating Gaussian random processes with specified spectra, *Comput. Sci. Stat.*, *24*, 534–534.

Pope, S. B. (2000), *Turbulent Flows*, Cambridge Univ. Press, Cambridge, U. K.

Rogers, L. T. (1998), Demonstration of an efficient boundary layer parameterization for unbiased propagation estimation, *Radio Sci.*, *33*(6), 1599–1608.

Rosenberg, A. P. (1999), A new rough surface parabolic equation program for computing low-frequency acoustic forward scattering from the ocean surface, *J. Acoust. Soc. Am.*, *105*(1), 144–153.

Rouseff, D. (1991), Simulating radar propagation through atmospheric turbulence using the tropospheric electromagnetic parabolic equation routine (temper), *Tech. Rep. JHU/APL-TG-1381, DTIC Doc.*, John Hopkins Univ. Applied Physics Lab., Laurel, Md.

Rouseff, D. (1992), Simulated microwave propagation through tropospheric turbulence, *IEEE Trans. Antennas Propag.*, *40*(9), 1076–1083, doi:10.1109/8.166533.

Tappert, F. D. (1977), The parabolic approximation method, in *Wave Propagation and Underwater Acoustics*, edited by J. B. Keller and J. S. Papadakis, pp. 224–287, Springer, Berlin.

Tatarskii, V. I. (1971), *The Effects of the Turbulent Atmosphere on Wave Propagation*, Israel Prog. for Sci. Trans., Jerusalem.

Wang, Y., D. Miller, D. Anderson, R. Cionco, and J. Lin (1992), A spatial length scale analysis of turbulent temperature and velocity fluctuations within and above an orchard canopy, *Boundary Layer Meteorol.*, *59*(1–2), 125–139.

Wesely, M. L. (1976), The combined effect of temperature and humidity fluctuations on refractive index, *J. Appl. Meteorol.*, *15*(1), 43–49.

Wilson, D. K., J. G. Brasseur, and K. E. Gilbert (1999), Acoustic scattering and the spectrum of atmospheric turbulence, *J. Acoust. Soc. Am.*, *105*(1), 30–34.

Wyngaard, J. C., and M. A. LeMone (1980), Behavior of the refractive index structure parameter in the entraining convective boundary layer, *J. Atmos. Sci.*, *37*(7), 1573–1585, doi:10.1175/1520-0469(1980)037<1573:BOTRIS>2.0.CO;2.

Yardim, C., P. Gerstoft, and W. S. Hodgkiss (2006), Estimation of radio refractivity from radar clutter using Bayesian Monte Carlo analysis, *IEEE Trans. Antennas Propag.*, *54*(4), 1318–1327, doi:10.1109/tap.2006.872673.

Yardim, C., P. Gerstoft, and W. S. Hodgkiss (2007), Statistical maritime radar duct estimation using hybrid genetic algorithm–Markov chain Monte Carlo method, *Radio Sci.*, *42*, RS3014, doi:10.1029/2006RS003561.

Yardim, C., P. Gerstoft, and W. S. Hodgkiss (2009), Sensitivity analysis and performance estimation of refractivity from clutter techniques, *Radio Sci.*, *44*, RS1008, doi:10.1029/2008RS003897.